A Full-Wave Electromagnetic Model for the Waveguide-to-Strip-Line Coupler Using Vias for Confinement of Parallel-Plate Modes

Allan Østergaard

***Abstract*—This paper presents a practical waveguide-to-strip-line coupler. An accurate integral-equation model satisfying all boundary conditions for the electromagnetic fields and all edge conditions for the currents are described. The integral equations are solved using the method of moments. An experimental –5-dB coupler has been built. Measured and computed scattering parameters are in excellent agreement. The waveguide-to-strip-line coupling terms agrees within 0.1 dB at the resonance frequency. The discussion and the presented data provides physical insight to the operation of the coupler itself.**

***Index Terms*—Coupler, integral equation, slot, strip line, waveguide.**

I. Introduction

THE gain of large microstrip antenna arrays has a maximum at a finite aperture size. This maximum arises at a certain aperture size where the increase in electric and dielectric losses with aperture size begins to exceed the increase in directivity [1]. For large microstrip antenna arrays, hybrid solutions where a low-loss transmission technology is applied for the primary level of the beam-forming network are often used.

Coupling between similar and dissimilar transmission lines through apertures has been a subject of interest since Bethe first published his theory of diffraction by small holes in 1944 [2].

In this paper, we shall study the coupling between a rectangular waveguide and a strip line through a slot. A similar geometry was first studied by Perini and Sferrazza in 1957 [3]. One characteristic that seems not to have caused much interest is that the slot tends to excite parallel-plate modes between the ground planes enclosing the strip line. As these modes may carry the majority of the coupled power away, the coupler becomes impractical. To prevent this, a number of vias between the two ground planes are added in the vicinity of the slot and along the strip line.[1] An outline of the coupler is shown in Fig. 1.

The purpose of the vias is to confine the power of the parallel-plate modes and to increase the coupling level by enclosing the aperture facing the strip-line region in a cavity. The vias located along the strip line serves to build a short section of waveguide operating below cutoff. Thus, power is restricted to enter/leave the cavity through the slot or along the strip line.

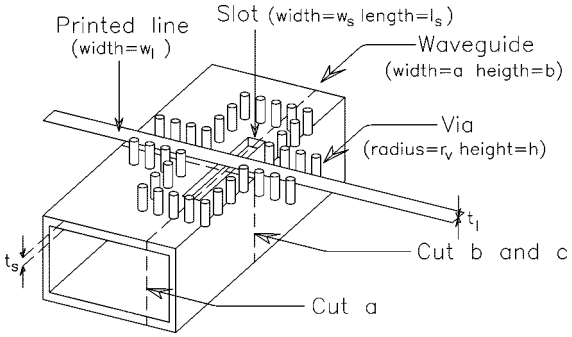

Fig. 1. Outline of the waveguide-to-strip-line coupler. The ground planes (shorted by the vias) and dielectric layers (supporting the strip line) are not shown.

As the waveguide may extend across an antenna array, multiple use of the coupler can be used for generating a sought for antenna aperture distribution in one dimension while simultaneously providing a low-loss feed mechanism.

We appreciate that the coupler is simple from a manufacturing and a mechanical point-of-view as self supporting wires and/or printed lines in the interior of the waveguide are avoided.

We appreciate that the coupler is a four-port. In order to analyze the coupler, we shall derive a set of coupled integral equations. The integral equations will be solved using the method of moments applying Galerkin testing. The reaction integrals will be formulated in the spatial domain for the waveguide and slot regions, while the strip line and vias region will be formulated in the spectral domain.

The scattering parameters for the coupling obtained by numerical means are validated against experimental results. In this paper, the $e^{j\omega t}$ time definition is applied.

II. Theory

In this section, the theoretical background for the numerical solution of the coupler is given.

The waveguide will be considered infinitely long and with perfectly conducting boundaries. The strip line will be embedded in a finite number of dielectric layers, each of finite thickness and each with a complex dielectric constant. The strip line will be considered infinitely long, perfectly conducting, and of zero thickness. The vias will be considered perfectly conducting. We shall analyze the slot as a short section of

Manuscript received July 21, 1998. This work was supported by the Danish Technical Research Council under Grant 9 400 274 and by TERMA Elektronik AS, Denmark.

The author is with TERMA Elektronik AS, DK-8520 Lystrup, Denmark (e-mail: aog@terma.dk).

Publisher Item Identifier S 0018-9480(00)00850-4.

[1]Subsequent to the submission of this paper, an analysis of a similar geometry was published by Kassner and Menzel [4].

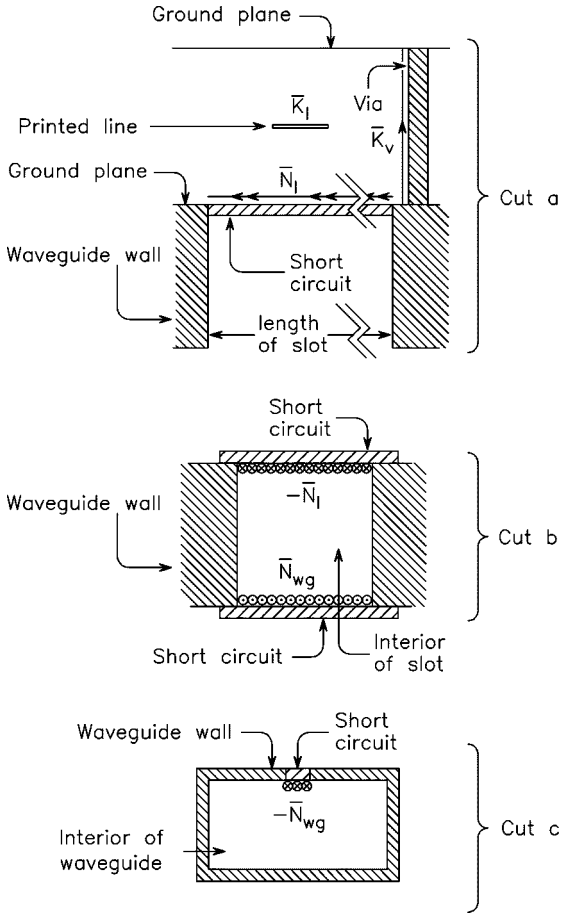

Fig. 2. Geometry of the waveguide-to-strip-line coupler. Cut a, b, and c (see Fig. 1) show three separate regions with magnetic currents and shorted apertures, as required by the equivalence principle.

waveguide. In Fig. 1, the symbols defining the geometry of the coupler are indicated.

A. Decomposition of the Coupler Problem

For the analysis, we shall divide the waveguide-to-strip-line coupler in three separate regions using the left-hand side and right-hand side half-space equivalence principle [5]. The result is shown in Fig. 2. The coupling between the three regions is accomplished by a set of magnetic currents located in the shorted apertures. The magnetic currents ensures the continuity of the tangential electric field across the apertures, while the continuity of the magnetic field is enforced by a set of coupled integral equations. With this procedure, the combined solution of the three regions are equivalent with the solution to the original problem.

We shall use three different coordinate systems, one for each of the three regions (see Fig. 3).

The following relations between the coordinates apply:

$$(x_{\rm wg}, y_{\rm wg}, z_{\rm wg}) = \left(-y_s + d + \frac{w_s}{2}, -z_s - t_s, x_s - \frac{l_s}{2}\right) \quad (1)$$

$$(x_l, y_l, z_l) = \left(-y_s + \frac{w_s}{2}, x_s - \frac{l_s}{2}, z_s\right) \quad (2)$$

where d is the $x_{\rm wg}$ coordinate of the slot center.

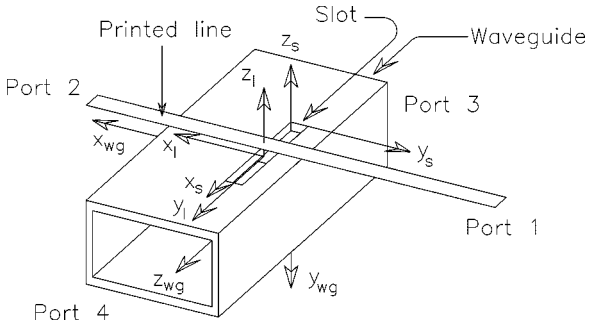

Fig. 3. Coordinate systems and numbering of coupler ports.

We shall apply a local circular cylindrical coordinate system $(r, \theta, z = z_l)$ for each via and the global Cartesian coordinate system (x_l, y_l, z_l) for all vias. The centers of the vias are defined by their coordinates in the Cartesian coordinate system, i.e., $(x_l, y_l) = (x_v, y_v)$.

B. Derivation and Discussion of the Integral Equations

The integral equations for tangential components of the relevant fields in the three regions of Fig. 2 may be written as

$$\bar{H}_{\rm wg} = \iint \bar{\bar{G}}_{\rm wg}^{HN}(-\bar{N}_{\rm wg})\, ds' + \bar{H}_{\rm wg}^{\rm inc} \quad (3)$$

$$\bar{H}_s = \iint \bar{\bar{G}}_s^{HN(-t_s)} \bar{N}_{\rm wg}\, ds' + \iint \bar{\bar{G}}_s^{HN(0)}(-\bar{N}_l)\, ds' \quad (4)$$

$$\bar{H}_l = \iint \bar{\bar{G}}_l^{HN} \bar{N}_l\, ds' + \iint \bar{\bar{G}}_l^{HK} \left(\bar{K}_l^{\rm inc} + \bar{K}_l^{\rm scat}\right) ds' + \iiint \bar{\bar{G}}_l^{HK} \sum_{v=1}^{V} \bar{K}_v\, dv' \quad (5)$$

$$\bar{E}_l = \iint \bar{\bar{G}}_l^{EN} \bar{N}_l\, ds' + \iint \bar{\bar{G}}_l^{EK} \left(\bar{K}_l^{\rm inc} + \bar{K}_l^{\rm scat}\right) ds' + \iiint \bar{\bar{G}}_l^{EK} \sum_{v=1}^{V} \bar{K}_v\, dv' \quad (6)$$

where wg denote the waveguide region, s the slot region, l the strip line region, and V the number of vias. Note that (6) defines the electric field on the strip line and vias.

In (3)–(6), seven Green's dyadics appear. We shall discuss these below.

1) Green's Dyadic for the Waveguide Region: The $\bar{\bar{G}}_{\rm wg}^{HN}$ links the magnetic field in the waveguide to a magnetic current source in the waveguide. For $x_{\rm wg}$ and $y_{\rm wg}$ directed magnetic currents, the Green's functions being part of the Green's dyadic may be derived by expanding the fields of the waveguide in TE and TM modes. For $z_{\rm wg}$ directed magnetic currents, this method unfortunately fails. Therefore, the Green's function has been derived using an intermediate electric vector potential $\bar{F}$. We find

$$\bar{F} = \varepsilon_0 \iiint_{V_N} \bar{\bar{G}}^{FN}(\bar{r} \mid \bar{r}') \cdot \bar{N}(\bar{r}')\, dv' \quad (7)$$

where the volume V_N contains the magnetic sources. The intermediate $\bar{\bar{G}}^{FN}$ dyad for the electric vector potential from a magnetic current may be expressed in the following form [6]:

$$\begin{aligned}\bar{\bar{G}}^{FN}&(\bar{r}\mid\bar{r}')\\ &=\sum_{m=0}^{\infty}\sum_{n=0}^{\infty}\frac{\gamma_m\gamma_n}{2jabk_z}\exp[-jk_z|z-z'|]\\ &\quad\left(\hat{x}\hat{x}\sin\left(\frac{m\pi}{a}x\right)\sin\left(\frac{m\pi}{a}x'\right)\cos\left(\frac{n\pi}{b}y\right)\cos\left(\frac{n\pi}{b}y'\right)\right.\\ &\quad+\hat{y}\hat{y}\cos\left(\frac{m\pi}{a}x\right)\cos\left(\frac{m\pi}{a}x'\right)\sin\left(\frac{n\pi}{b}y\right)\sin\left(\frac{n\pi}{b}y'\right)\\ &\quad\left.+\hat{z}\hat{z}\cos\left(\frac{m\pi}{a}x\right)\cos\left(\frac{m\pi}{a}x'\right)\cos\left(\frac{n\pi}{b}y\right)\cos\left(\frac{n\pi}{b}y'\right)\right)\end{aligned}\tag{8}$$

where

$$\gamma_0=1\quad\gamma_1=\gamma_2=\cdots=2.\tag{9}$$

Note that the (m,n) terms of (8) neither indicate TE_{mn} nor TM_{mn} modes. Rather, (8) is a representation of the complete field. The electric and magnetic fields may be computed using the relations

$$\bar{E}=-\frac{1}{\varepsilon_0}\nabla\times\bar{F}\tag{10}$$

and

$$\bar{H}=-j\omega\bar{F}+\frac{\nabla\nabla\cdot\bar{F}}{j\omega\mu_0\varepsilon_0}.\tag{11}$$

Hence,

$$\bar{\bar{G}}_{\mathrm{wg}}^{HN}=\frac{1}{jk_0\eta_0}\left(k_0^2+\nabla\nabla\cdot\right)\bar{\bar{G}}_{\mathrm{wg}}^{FN}\tag{12}$$

2) Green's Dyadics for the Slot Region: The $\bar{\bar{G}}_s^{HN(-t_s)}$ and $\bar{\bar{G}}_s^{HN(0)}$ links the magnetic field in a shorted section of a waveguide, i.e., the slot with the planar magnetic sources located in front of its shorted apertures.

3) Green's Dyadics for the Line Region: The $\bar{\bar{G}}_l^{HN}$, $\bar{\bar{G}}_l^{HK}$, $\bar{\bar{G}}_l^{EN}$, and $\bar{\bar{G}}_l^{EK}$ all pertain to the line region. In this region, the Green's functions cannot be derived in closed form in the spatial domain. Furthermore, since the region is unbounded in at least two dimensions, the Green's dyadics will not be given as a sum of discrete modes, but rather as a continuous spectrum of modes.

One may obtain the Green's dyadics in the spatial domain by numerical computation of the double inverse Fourier transform of their spectral-domain counterparts [7].

In this paper, we shall apply a different formulation where the integral equations are discretized in the spectral domain. It is important to note that a spatial-domain formulation and a spectral-domain formulation gives identical results when applied for the same problem.

Although the spectral-domain Green's dyadics for a general multilayered medium linking the electromagnetic fields with its electric and magnetic sources can be derived in closed form, it will not be done in this paper. Instead, a formulation in which the spectral-domain Green's dyadics are computed numerically [8] will be used.

For those of the inner products, defined in Section II-D, which involve the vias, the work of [8] have been augmented in order to allow analytical integration in the z-direction, i.e., along the surface of the vias.

C. Expansion of Currents and Fields

1) Incident and Scattered Fields in the Waveguide: For the waveguide, we shall apply an expansion of TE and TM waveguide modes normalized as described in [9, Sec. 8.1].

We shall assume that the only mode propagating unattenuated (not considering losses) is the TE_{10} mode and that all other modes are below cutoff. For the incident field $\bar{H}_{\mathrm{wg}}^{\mathrm{inc}}$ in (3), we shall, therefore, apply the magnetic field of the TE_{10} mode. The voltage of its electric-field mode vector is set to 1 V. Hence, the complex voltages of the TE_{10} modes scattered from the slot in either directions of the waveguide give the scattering parameters for the waveguide part.

2) Expansion of Aperture Fields in the Slot: In general, the electric field in either ends of a waveguide is given by a sum of all TE and TM modes. In this paper, we shall assume that the slots are in the order of one-half free-space wavelength long and that their width are small compared to the free-space wavelength. Further, we shall restrict the analysis to rectangular slots.

In view of the slot size, one may reduce the number of modes necessary for representing the electric field in the slot to TE_{q0} $(q=1,2,\cdots)$ modes only. In terms of a representation of the equivalent magnetic currents located in the apertures of the slot, i.e., $\bar{N}_{\mathrm{wg}}$ and $-\bar{N}_l$ of Fig. 2 we, therefore, obtain

$$\bar{N}_{\mathrm{wg}}=\sum_{q=1}^{Q}V_q^{\mathrm{wg}}\left(\bar{e}_{q0}^{e}\times\hat{z}_s\right)=\sum_{q=1}^{Q}V_q^{\mathrm{wg}}\bar{m}_q\tag{13}$$

$$\bar{N}_l=\sum_{q=1}^{Q}V_q^{l}\left(\bar{e}_{q0}^{e}\times\hat{z}_s\right)=\sum_{q=1}^{Q}V_q^{l}\bar{m}_q\tag{14}$$

where Q is the upper limit, which truncates the expansion of the magnetic current. Q must be selected sufficiently large in order to ensure that the electric field can always be accurately modeled. In case of a slot, a conservative choice for Q is the nearest integer of l_s/w_s. A practical limit of Q is somewhat lower as the modes corresponding to increasing values of Q becomes strongly evanescent. The V_q's are the unknown weights and the electric $\bar{e}_{q0}^{e}$ and magnetic $\bar{h}_{q0}^{e}$ mode vectors (and their longitudinal components) of the TE field are given by

$$\bar{e}^{e}(x,y)=\hat{z}_s\times\nabla_t\psi^{e}(x,y)\tag{15}$$

$$e_z^{e}(x,y)=0\tag{16}$$

$$\bar{h}^{e}(x,y)=-\nabla_t\psi^{e}(x,y)\tag{17}$$

$$h_z^{e}(x,y)=\mp j\frac{k^2-k_z^2}{k_z}\psi^{e}(x,y)\tag{18}$$

Further, the eigenfunctions $\psi^{e}(x,y,z)$ is a solution to $(\nabla^2+k^2)\psi^{e}(x,y,z)=0$ [9, p. 387]. For the rectangular

waveguide, the boundary condition for the TE field in terms of ψ^e is $\partial\psi^e/\partial n = 0$. For the transverse dependence, we obtain

$$\psi^e_{mn}(x,y) = \frac{1}{\pi}\sqrt{\frac{l_s w_s \gamma_m \gamma_n}{(mb)^2+(na)^2}}\cos\left(\frac{m\pi}{l_s}x_s\right)\cos\left(\frac{n\pi}{w_s}y_s\right) \tag{19}$$

where γ_m and γ_n satisfy (9).

3) Expansion of Currents on the Strip Line: For the strip line, we shall apply an expansion of the electric surface current. The current will be modeled by incident, reflected, and transmitted waves. For these waves, we shall assume a longitudinal dependence of $e^{\mp jk_e x}$. In order to determine the propagation constant k_e, we shall analyze the strip line with neither the presence of the aperture nor the vias, using a method similar to the one in [10]. Using this method, the transverse dependence of the current is also determined. For future reference we shall denote the y dependence of the x-directed current as $k_{l,x}(y)$. Hence, $k_{l,x}(y)$ will be a weighted sum of so-called Maxwellian expansion functions [11].

In order to model the strip-line current in the proximity of the aperture, we shall include a number of piecewise sinusoidal modes (PWS) in the expansion. The incident, reflected, and transmitted modes are

$$\bar{K}^{\text{inc}} = \hat{x}\Big(f_{\cos}(x) - jf_{\sin}(x)\Big)k_{l,x}(y) \tag{20}$$

$$\bar{K}^{\text{ref}} = \hat{x}\Big(f_{\cos}(x) + jf_{\sin}(x)\Big)k_{l,x}(y) \tag{21}$$

$$\bar{K}^{\text{tr}} = \hat{x}\Big(f^t_{\cos}(x) - jf^t_{\sin}(x)\Big)k_{l,x}(y) \tag{22}$$

where

$$f_{\sin} = \begin{cases}\sin(k_e x), & \text{if } -M\pi \le k_e x \le 0\\ 0, & \text{elsewhere}\end{cases} \tag{23}$$

$$f_{\cos} = \begin{cases}\cos(k_e x), & \text{if } -M\pi - \dfrac{\pi}{2} \le k_e x \le -\dfrac{\pi}{2}\\ 0 & \text{elsewhere}\end{cases} \tag{24}$$

$$f^t_{\sin} = \begin{cases}\sin(k_e x), & \text{if } 0 \le k_e x \le M\pi\\ 0, & \text{elsewhere}\end{cases} \tag{25}$$

$$f^t_{\cos} = \begin{cases}\cos(k_e x), & \text{if } \dfrac{\pi}{2} \le k_e x \le M\pi + \dfrac{\pi}{2}\\ 0, & \text{elsewhere.}\end{cases} \tag{26}$$

For a discussion of the parameter M, the reader is referred to [12]. M is chosen to be an integer $M \ge 4$.

The PWS modes are

$$\bar{K}^{\text{PWS}} = \sum_{i=1}^{I} I_i \bar{f}_i \tag{27}$$

$$\begin{aligned}\bar{f}_i &= \hat{x} f_i^{\text{PWS}}(x) k_{l,x}(y)\\ &= \hat{x}\frac{\sin\Big(k_e(h_i - |x - x_i|)\Big)}{\sin(k_e h_i)}k_{l,x}(y)\end{aligned} \tag{28}$$

where h_i is the half width of the ith PWS mode and x_i its center.

Hence, the strip-line current may be written

$$\begin{aligned}\bar{K}_l &= \bar{K}_l^{\text{inc}} + \bar{K}_l^{\text{scat}}\\ &= \bar{K}_l^{\text{inc}} - R\bar{K}^{\text{ref}} + T\bar{K}^{\text{tr}} + \sum_{i=1}^{I} I_i \bar{f}_i.\end{aligned} \tag{29}$$

4) Expansion of Currents on the Vias: We may think of a via as a circular cylinder connecting the two ground planes enclosing the strip line. In this paper, we shall assume that the radius of a via is small in terms of guided wavelengths in the dielectric layers surrounding the via. At this point, we, therefore, assume that the current on the surface of a via is dependent of the z coordinate only.

In order to select an expansion for the currents on the vias, we need to investigate the behavior of the current flowing on a via embedded by a number of dielectric layers with different thicknesses and dielectric constants.

Abusing the notation somewhat, we may write the current flowing on the surface of via v as

$$\bar{K}_v(r,\theta,z) = \frac{\hat{z}}{2\pi r_v}\delta(r - r_v)K_v(z) \tag{30}$$

where r_v is the radius of the via and δ is the Dirac delta function.

Using the continuity equation for the via current, the boundary condition for the displacement flux vector normal to the surface of a via, and the boundary condition for the electric field at an interface between adjacent dielectric layers $z = z^{\text{int}}$ embedding a via, we obtain

$$\frac{1}{\varepsilon_r^+}\frac{\partial K_v(z = z^{+\text{int}})}{\partial z} = \frac{1}{\varepsilon_r^-}\frac{\partial K_v(z = z^{-\text{int}})}{\partial z} \tag{31}$$

where $z^{+\text{int}}$ and $z^{-\text{int}}$ denote positions infinitesimally above and below z^{int}, respectively. As the derivative of K_v is discontinuous across the interface between two dielectric layers, it is not feasible to expand the z-dependent current on a via into a set of entire domain modes. Therefore, the following expansion is chosen for the current on via v:

$$\begin{aligned}\bar{K}_v(r,\theta,z) &= \sum_{l=1}^{L}\sum_{m=0}^{M} C_{vlm}\bar{K}_{vlm}(r,\theta,z)\\ &= \frac{\hat{z}}{2\pi r_v}\delta(r - r_v)\sum_{l=1}^{L}\sum_{m=0}^{M} C_{vlm}K_{vlm}(z)\end{aligned} \tag{32}$$

where

$$K_{vlm}(z) = \begin{cases}\cos\left(\frac{m\pi}{h}z\right), & \text{if } z \in \text{layer no. } l\\ 0, & \text{otherwise}\end{cases} \tag{33}$$

where C_{vlm} is a complex weight (constant) for the mth expansion function in layer l and h is the distance between the ground planes enclosing the strip line. We appreciate that $\partial K_v(z)/\partial z = 0$ is satisfied at the surface of the two ground planes.

The current on a via must be continuous and (31) must be satisfied. Therefore, we may impose the following conditions between the weights of the expansion functions for the z

dependence of the via current at the interface ($z = z^{\rm int}$) between two neighboring dielectric layers:

$$\sum_{m=0}^{M} C_{vlm}\cos\left(\frac{m\pi}{h}z^{\rm int}\right) = \sum_{m=0}^{M} C_{v(l+1)m}\cos\left(\frac{m\pi}{h}z^{\rm int}\right) \quad (34)$$

$$\sum_{m=0}^{M} \frac{mC_{vlm}}{\varepsilon_{rl}}\sin\left(\frac{m\pi}{h}z^{\rm int}\right) = \sum_{m=0}^{M} \frac{mC_{v(l+1)m}}{\varepsilon_{r(l+1)}}\sin\left(\frac{m\pi}{h}z^{\rm int}\right). \quad (35)$$

We appreciate that (34) and (35) define a set of relations between the expansion modes on the vias that enforces the proper behavior of the current and charge distribution along the surface of the vias.

5) Substituting the Unknown Currents: In (3)–(6), the incident magnetic field $H_{\rm wg}^{\rm inc}$ in the waveguide and the incident current $K_l^{\rm inc}$ on the strip line are assumed known. Substituting the aperture currents $\bar{m}_q$'s, the line current $\bar{K}^{\rm ref}, \bar{K}^{\rm tr}$, and $\bar{f}_i$, and the current on the vias $\bar{K}^{vlm}$ using (13), (14), (29), and (32), respectively, yields four equations with $2Q+I+2+VL(M+1)$ unknown (complex) expansion coefficients $V_q^{\rm wg}, V_q^l, R, T, I_i$, and C_{vlm}.

D. Enforcing the Boundary Conditions and Weighting the Integral Equations

In order to obtain a quadratic linear system of equations in the unknown expansion coefficients, the continuity of the magnetic field across the two apertures and a zero tangential electric field on the strip line and the vias is enforced. Thus, the equations obtained are discretized using the Galerkin method.

We introduce the notation in (36) in order to define an inner product between a field quantity $\bar{B}$ and a weight function $\bar{W}$ in terms of a surface (or volume) integral in field point coordinates

$$\langle \bar{W}, \bar{B}\rangle = \iint_{\substack{\rm Domain\\ \rm of W}} \bar{W}\cdot\bar{B}\,ds = \iiint_{\substack{\rm Domain\\ \rm of W}} \bar{W}\cdot\bar{B}\,dv. \quad (36)$$

1) The Aperture Facing the Main Waveguide: In the aperture ($z_s = -t_s$) facing the main waveguide, we shall weight the magnetic field (3) and (4) using the magnetic current $\bar{m}_p$, defined in (13). We obtain

$$\sum_{q=1}^{Q} V_q^{\rm wg}(y_{\rm wg}^{pq} + y_s^{pq}) + \sum_{q=1}^{Q} V_q^l y_t^{pq} = i_s^p \quad (37)$$

where

$$y_{\rm wg}^{pq} = \left\langle \bar{m}_p, \iint \bar{\bar{G}}_{\rm wg}^{HN}(-\bar{m}_q)\,ds'\right\rangle \quad (38)$$

$$y_s^{pq} = \left\langle -\bar{m}_p, \iint \bar{\bar{G}}_s^{HN(-t_s)}\bar{m}_q\,ds'\right\rangle \quad (39)$$

$$y_t^{pq} = \left\langle -\bar{m}_p, \iint \bar{\bar{G}}_s^{HN(0)}(-\bar{m}_q)\,ds'\right\rangle \quad (40)$$

$$i_s^p = \left\langle -\bar{m}_p, \bar{H}_{\rm wg}^{\rm inc}\right\rangle. \quad (41)$$

We shall denote $y_{\rm wg}^{pq}$ the waveguide self admittance, y_s^{pq} the slot self admittance, and y_t^{pq} the slot transfer admittance.

2) The Aperture Facing the Strip Line: In the aperture ($z_s = 0$) facing the strip line, we shall weight the magnetic field (4) and (5) using the magnetic current $\bar{m}_p$ defined in (14). We obtain

$$\sum_{q=1}^{Q} V_q^{\rm wg} y_t^{pq} + \sum_{q=1}^{Q} V_q^l\,(y_s^{pq} + y_l^{pq}) - R\beta^{p,\rm ref} + T\beta^{p,\rm tr} + \sum_{i=1}^{I} I_i\beta^{p,i} + \sum_{v=1}^{V}\sum_{l=1}^{L}\sum_{m=0}^{M} C_{vlm}\beta^{p,vlm} = i_l^p \quad (42)$$

where

$$y_l^{pq} = \left\langle -\bar{m}_p, \iint \bar{\bar{G}}_l^{HN}\bar{m}_q\,ds'\right\rangle \quad (43)$$

$$y_s^{pq} = \left\langle \bar{m}_p, \iint \bar{\bar{G}}_s^{HN(0)}(-\bar{m}_q)\,ds'\right\rangle \quad (44)$$

$$y_t^{pq} = \left\langle \bar{m}_p, \iint \bar{\bar{G}}_s^{HN(-t_s)}\bar{m}_q\,ds'\right\rangle \quad (45)$$

$$\beta^{p,\rm ref} = \left\langle -\bar{m}_p, \iint \bar{\bar{G}}_l^{HK}\bar{K}^{\rm ref}ds'\right\rangle \quad (46)$$

$$\beta^{p,\rm tr} = \left\langle -\bar{m}_p, \iint \bar{\bar{G}}_l^{HK}\bar{K}^{\rm tr}ds'\right\rangle \quad (47)$$

$$\beta^{p,i} = \left\langle -\bar{m}_p, \iint \bar{\bar{G}}_l^{HK}\bar{f}_i\,ds'\right\rangle \quad (48)$$

$$\beta^{p,vlm} = \left\langle -\bar{m}_p, \iiint \bar{\bar{G}}_l^{HK}\bar{K}_{vlm}dv'\right\rangle \quad (49)$$

$$i_l^p = \left\langle \bar{m}_p, \iint \bar{\bar{G}}_l^{HK}\bar{K}_l^{\rm inc}\,ds'\right\rangle. \quad (50)$$

3) The Strip Line: On the strip line, we shall deviate from the strict use of the Galerkin method of moments procedure. The justification is that $\bar{K}^{\rm ref}$ and $\bar{K}^{\rm tr}$ are not suited as weight functions. Both $\bar{K}^{\rm ref}$ and $\bar{K}^{\rm tr}$ are derived from a solution of the infinite strip-line problem. Hence, the boundary conditions for the electric field on the strip line are automatically satisfied when considering $\bar{K}^{\rm ref}$ and $\bar{K}^{\rm tr}$ as expansion functions (sources) for the field. Hence, two additional weight functions are required for obtaining a quadratic linear system of equations in the unknown expansion coefficients (see Fig. 4). Weighting the electric field (6) on the strip line yields

$$\sum_{q=1}^{Q} V_q^l\mu^{r,q} - Rz^{r,\rm ref} + Tz^{r,\rm tr} + \sum_{i=1}^{I} I_i z^{r,i} + \sum_{v=1}^{V}\sum_{l=1}^{L}\sum_{m=0}^{M} C_{vlm}z^{r,vlm} = v_l^r \quad (51)$$

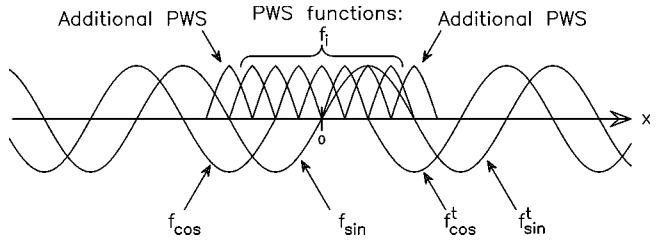

Fig. 4. Expansion (and weight) functions on the strip line.

where

$$\mu^{r,q} = \left\langle \bar{f}_r, \iint \bar{\bar{G}}_l^{EN} \bar{m}_q \, ds' \right\rangle \tag{52}$$

$$z^{r,\mathrm{ref}} = \left\langle \bar{f}_r, \iint \bar{\bar{G}}_l^{EK} \bar{K}^{\mathrm{ref}} \, ds' \right\rangle \tag{53}$$

$$z^{r,\mathrm{tr}} = \left\langle \bar{f}_r, \iint \bar{\bar{G}}_l^{EK} \bar{K}^{\mathrm{tr}} \, ds' \right\rangle \tag{54}$$

$$z^{r,i} = \left\langle \bar{f}_r, \iint \bar{\bar{G}}_l^{EK} \bar{f}_i \, ds' \right\rangle \tag{55}$$

$$z^{r,vlm} = \left\langle \bar{f}_r, \iiint \bar{\bar{G}}_l^{EK} \bar{K}_{vlm} \, dv' \right\rangle \tag{56}$$

$$v_l^r = \left\langle \bar{f}_r, - \iint \bar{\bar{G}}_l^{EK} \bar{K}_l^{\mathrm{inc}} \, ds' \right\rangle. \tag{57}$$

4) The Vias: On the vias, we shall weight the electric field (6) using the expansion for the electric current $\bar{K}_{vlm}$ in (32). We obtain

$$\sum_{q=1}^{Q} V_q^l \mu^{s,q} - R z^{s,\mathrm{ref}} + T z^{s,\mathrm{tr}} + \sum_{i=1}^{I} I_i z^{s,i} + \sum_{v=1}^{V} \sum_{l=1}^{L} \sum_{m=0}^{M} C_{vlm} z^{s,vlm} = v_l^s \tag{58}$$

where

$$\mu^{s,q} = \left\langle \bar{K}_s, \iint \bar{\bar{G}}_l^{EN} \bar{m}_q \, ds' \right\rangle \tag{59}$$

$$z^{s,\mathrm{ref}} = \left\langle \bar{K}_s, \iint \bar{\bar{G}}_l^{EK} \bar{K}^{\mathrm{ref}} ds' \right\rangle \tag{60}$$

$$z^{s,\mathrm{tr}} = \left\langle \bar{K}_s, \iint \bar{\bar{G}}_l^{EK} \bar{K}^{\mathrm{tr}} ds' \right\rangle \tag{61}$$

$$z^{s,i} = \left\langle \bar{K}_s, \iint \bar{\bar{G}}_l^{EK} \bar{f}_i \, ds' \right\rangle \tag{62}$$

$$z^{s,vlm} = \left\langle \bar{K}_s, \iiint \bar{\bar{G}}_l^{EK} \bar{K}_{vlm} \, dv' \right\rangle \tag{63}$$

$$v_l^s = \left\langle \bar{K}_s, - \iint \bar{\bar{G}}_l^{EK} \bar{K}_l^{\mathrm{inc}} \, ds' \right\rangle \tag{64}$$

where $\bar{K}_s, s \in \{1, \cdots, VL(M+1)\}$ denotes one of the weighting modes (identical to the expansion modes (32) as we apply the Galerkin technique).

At this point, it should be noted that part of the equations obtained from (58) may be replaced by the current/charge relations for the via current in (34) and (35). Care should be taken in order to avoid that linear dependent equations are introduced into the matrix equation for the full method-of-moments solution.

E. Method-of-Moments Matrix for the Coupler Problem

By means of the Galerkin method, with the small modifications of two additional PWS functions on the strip line, we have obtained (37), (42), (51), and (58). We may write these in matrix form (65), shown at the bottom of this page. Solving (65) yields the scattering parameters on the strip line. In order to obtain the reflected and transmitted modes in the main waveguide, we need to consider $-\bar{N}_{\mathrm{wg}} = -\sum V_q^{\mathrm{wg}} \bar{m}_q$ radiating into the interior of the main waveguide. We shall treat this problem in Section II-F. We shall treat the numerical computation of the elements of (65) below. Most of the elements concerned with the waveguide and slot can be derived in closed form. These are y_{wg}^{pq}, y_s^{pq}, y_t^{pq}, and i_s^p.

1) The Waveguide Self Admittance: For the waveguide self admittance (38), using (12) and (13), we obtain

$$y_{\mathrm{wg}}^{pq} = \frac{1}{k_0 \eta} \frac{4a}{\pi^2 l_s w_s b} \sum_{n=0}^{\infty} \sum_{m=0}^{\infty} \frac{\gamma_n \gamma_m \cos^2 \frac{m\pi d}{a} \sin^2 \frac{m\pi w_s}{2a}}{m^2 k_z \left(\left(\frac{q\pi}{l_s} \right)^2 - k_z^2 \right)} (Q_1 + Q_2) \tag{66}$$

where γ_m and γ_n satisfy (9).

$$\begin{pmatrix} \vdots & \vdots & \vdots & \vdots & \vdots & \vdots \\ \cdots y_{\mathrm{wg}}^{pq} + y_s^{pq} \cdots & \cdots y_t^{pq} \cdots & 0 & 0 & \cdots 0 \cdots & \cdots 0 \cdots \\ \vdots & \vdots & \vdots & \vdots & \vdots & \vdots \\ \cdots y_t^{pq} \cdots & \cdots y_s^{pq} + y_l^{pq} \cdots & \beta^{p,\mathrm{ref}} & \beta^{p,\mathrm{tr}} & \cdots \beta^{p,i} \cdots & \cdots \beta^{p,vlm} \cdots \\ \vdots & \vdots & \vdots & \vdots & \vdots & \vdots \\ \cdots 0 \cdots & \cdots \mu^{r,q} \cdots & z^{r,\mathrm{ref}} & z^{r,\mathrm{tr}} & \cdots z^{r,i} \cdots & \cdots z^{r,vlm} \cdots \\ \vdots & \vdots & \vdots & \vdots & \vdots & \vdots \\ \cdots 0 \cdots & \cdots \mu^{s,q} \cdots & z^{s,\mathrm{ref}} & z^{s,\mathrm{tr}} & \cdots z^{s,i} \cdots & \cdots z^{s,vlm} \cdots \\ \vdots & \vdots & \vdots & \vdots & \vdots & \vdots \end{pmatrix} \begin{pmatrix} \vdots \\ V_q^{\mathrm{wg}} \\ \vdots \\ V_q^l \\ \vdots \\ -R \\ T \\ \vdots \\ I_i \\ \vdots \\ C_{vlm} \\ \vdots \end{pmatrix} = \begin{pmatrix} \vdots \\ i_s^p \\ \vdots \\ i_l^p \\ \vdots \\ v_l^r \\ \vdots \\ v_l^s \\ \vdots \end{pmatrix} \tag{65}$$

The Q_1 and Q_2 terms are given by

$$Q_1 = \frac{p\pi}{l_s}\frac{q\pi}{l_s}\frac{k_0^2 - k_z^2}{\left(\frac{p\pi}{l_s}\right)^2 - k_z^2}\Big(1 + \cos(p\pi)\cos(q\pi) - e^{-jk_z l_s}\big(\cos(p\pi) + \cos(q\pi)\big)\Big) \tag{67}$$

and

$$Q_2 = \begin{cases} 0, & \text{when } p \neq q \\ jk_z l_s\left(k_0^2 - \left(\frac{q\pi}{l_s}\right)^2\right), & \text{when } p = q. \end{cases} \tag{68}$$

2) The Slot Self Admittance: We appreciate that the slot self admittances y_s^{pq} given by (39) and (44) agree. The general result is

$$y_s^{pq} = \begin{cases} \dfrac{\cot(k_z t_s)}{jZ_{q0}^e}, & \text{when } p = q \\ 0, & \text{when } p \neq q. \end{cases} \tag{69}$$

3) The Slot Transfer Admittance: The slot transfer admittances y_t^{pq} given by (40) and (45) may be obtained using (13)–(15) and (17) as follows:

$$\begin{aligned} y_t^{pq} &= \left\langle -\bar{m}_p, \iint \bar{\bar{G}}_s^{HN(0)}(-\bar{m}_q)\, ds' \right\rangle \\ &= \left\langle -\bar{e}_{p0}^e, \bar{h}_{q0}^e \frac{1}{-jZ_{q0}^e}\sin(k_z t_s) \right\rangle \\ &= \begin{cases} \dfrac{-1}{jZ_{q0}^e \sin(k_z t_s)}, & \text{when } p = q \\ 0, & \text{when } p \neq q. \end{cases} \end{aligned} \tag{70}$$

4) The Current due to an Incident TE_{10} *Mode in the Main Waveguide:* In this paper, i_s^p is derived by combining the derivations of Section II-F with the reciprocity theorem

$$i_s^p = \begin{cases} -j\sqrt{\dfrac{4}{abl_s w_s}}\dfrac{4p\pi}{l_s k_0 \eta}\cos\left(\dfrac{\pi}{a}d\right)\sin\left(\dfrac{\pi w_s}{2a}\right)\dfrac{\cos\left(\frac{k_z l_s}{2}\right)}{\left(\frac{p\pi}{l_s}\right)^2 - k_z^2}, \\ \qquad \text{when } p \text{ is odd} \\ \pm\sqrt{\dfrac{4}{abl_s w_s}}\dfrac{4p\pi}{l_s k_0 \eta}\cos\left(\dfrac{\pi}{a}d\right)\sin\left(\dfrac{\pi w_s}{2a}\right)\dfrac{\sin\left(\frac{k_z l_s}{2}\right)}{\left(\frac{p\pi}{l_s}\right)^2 - k_z^2}, \\ \qquad \text{when } p \text{ is even.} \end{cases} \tag{71}$$

Note that the result depends of the propagation direction of the incident TE_{10} mode. The upper sign (when p is even) for i_s^p applies to incident waves propagating in the positive direction of the z axis and the lower sign to incident waves propagating in the negative direction of the z axis.

5) Inner Products Corresponding to the Coupling Between the Slot and Vias: The inner products corresponding to the coupling between the slot and vias are the $\mu^{s,q}$ and $\beta^{p,vlm}$ elements. (As a consequence of reciprocity, $\mu^{s,q} = -\beta^{p,vlm}$ when $vlm = s$ and $p = q$.)

Due to the techniques used for the numerical computation of the inner products, a direct integration of the electric field on a via (with a cylindrical surface) from the magnetic current (within a rectangular slot), i.e., $\mu^{s,q}$ or vice versa, i.e., $\beta^{p,vlm}$ is not feasible [5], [12].

For the $\mu^{s,q}$ and $\beta^{p,vlm}$ elements, we shall, therefore, apply the approximation that the currents on the vias are not cylindrical surface currents, but line currents located on the axis of the vias. The corresponding currents are defined as

$$\begin{aligned} \bar{K}_{vlm}(r,\theta,z) &= \lim_{r_v \to 0}\frac{\hat{z}}{2\pi r_v}\delta(r - r_v)K_{vlm}(z) \\ &= \hat{z}\delta(x - x_v)\delta(y - y_v)K_{vlm}(z) \end{aligned} \tag{72}$$

where the local cylindrical coordinates are assumed for each via, while global Cartesian coordinates are used with the centers of the vias located at x_v, y_v.

In order to maintain the reciprocity relation between $\mu^{s,q}$ and $\beta^{p,vlm}$, we shall test the electric field on a via along its center axis instead of on its surface.

The approximation of (72) holds when the radius of a via is small compared to the guided wavelength in the dielectric layers embedding the via.

6) Inner Products Corresponding to Self and Mutual Coupling Between Vias: The inner products corresponding to the self and mutual coupling between vias are the $z^{s,vlm}$ elements.

A direct integration of the electric field on a via (with a cylindrical surface) from its electric current, i.e., the self coupling, is possible [5]. However, a direct integration of the mutual terms are not possible.

Nevertheless, it is possible to compute the electric field, from the true cylindrical electric surface current on a via, along a line at a distance from the source, i.e., on the line defined by $\delta(r - r_E)\delta(\theta - \theta_E)$. As a consequence of the rotational symmetry of the geometry, the field shall be independent of θ_E.

In terms of the numerical effort, we save one integration, as the $d\theta$ integration may be performed analytically.

We may, therefore, compute the mutual coupling terms between a via (a) and a via (b) using the value of the electric field radiated from via (a) at a number of positions, i.e., $\delta(r - r_E)\delta(\theta - \theta_E)$, selected such that they encircle via (b). Interpolation has been applied as a mean for increasing the numerical efficiency. The surface integration of via (b) directly follows.

Hence, all elements of $z^{s,vlm}$ are computed numerically without approximation.

7) Inner Products Corresponding to the Coupling Between the Strip Line and Vias: The inner products corresponding to the coupling between the strip line and vias are the $z^{r,vlm}$ $z^{s,\mathrm{ref}}$, $z^{s,\mathrm{tr}}$, $z^{s,i}$, and v_l^s elements. (As a consequence of reciprocity, the elements of $z^{r,vlm} = z^{s,i}$ when $i = r$ and $vlm = s$.)

As a matter of simplification, we shall not compute any of these inner products. The electric field scattered or radiated of a symmetric strip line is antisymmetric with respect to the z-directed electric field along the axis of a via. The corresponding, i.e., antisymmetric, current on a via may be obtained from (33) with m odd. Although antisymmetric current on the vias will be

excited due to the presence of the slot, the coupling to the line is weak. The reason being twofold is as follows.

- The antisymmetric currents (corresponding to (33) with m odd) are expected to have much smaller amplitude than the symmetric current (corresponding to (33) with $m = 0$). Hence, their scattered/radiated field also have smaller amplitude.
- The field scattered/radiated from the symmetric current ($m = 0$) propagate as an unattenuated parallel-plate mode. The symmetric mode does not couple to the symmetric strip line.

The field scattered/radiated from the higher order currents on the vias, i.e., $m \in \{1, 2, \cdots\}$ propagate as evanescent parallel-plate modes. Hence, their attenuation ensures that the coupling to the strip line can be neglected.

Therefore, all elements of the $z^{r,vlm}$, $z^{s,\mathrm{ref}}$, $z^{s,\mathrm{tr}}$, $z^{s,i}$, and v_l^s inner products are set equal to zero.

8) Remaining Inner Products: For the remaining inner products, the inherent fourfold (spatial domain) integrals are reduced by analytical means to two-dimensional (spectral domain) integrals. No other option exists than performing these integrations by numerical computation [12].

F. Scattered Modes in the Waveguide

Once the magnetic current, i.e., the electric field in the slot aperture has been found, we need to determine the waves propagating in either direction of the main waveguide.

Assuming that all sources are magnetic and confined to a finite volume V, the reciprocity theorem [13, p. 128] reduces to

$$\int_V \bar{H}^b \cdot \bar{N}^a \, dV = \int_V \bar{H}^a \cdot \bar{N}^b \, dV \tag{73}$$

where $\bar{H}^a$ is the field to be determined and $\bar{N}^a = -\bar{N}_{\mathrm{wg}}$ is known from solving (65).

$\bar{N}^a$ is defined (in the waveguide coordinate system) by

$$\bar{N}^a = \hat{z}_{\mathrm{wg}} \sum_{q=1}^{Q} V_q^{\mathrm{wg}} \sqrt{\frac{2}{w_s l_s}} \sin\left(\frac{q\pi}{l_s}\left(z_{\mathrm{wg}} + \frac{l_s}{2}\right)\right). \tag{74}$$

Since $\bar{N}^a$ is solely z_{wg} directed, it does not support TM modes in the main waveguide. The three remaining quantities, i.e., $\bar{H}^a, \bar{N}^b$ and $\bar{H}^b$ will be formulated differently in the case of backward and forward scatterd waves in the main waveguide. We shall, therefore, treat these two cases independently.

In the remainder of this section, the subscripts of the Cartesian waveguide coordinates $(x_{\mathrm{wg}}, y_{\mathrm{wg}}, z_{\mathrm{wg}})$ will be suppressed. Hence, $x = x_{\mathrm{wg}}, y = y_{\mathrm{wg}}$, and $z = z_{\mathrm{wg}}$.

1) Scattered Waves in the Negative Direction of the z_{wg} Axis: With $\bar{H}^a$ unknown, we shall expand it into a sum of known waveguide modes $\bar{h}_{mn}$ with unknown coefficients I_{mn}^{e-}, propagating in the negative direction of the z_{wg} axis

$$\bar{H}^a = -\sum_{m=0}^{\infty} {\sum_{n=0}^{\infty}}' I_{mn}^{e-} \left(\bar{h}_{mn}^e + \hat{z} h_{z,mn}^e\right) e^{jk_z z}. \tag{75}$$

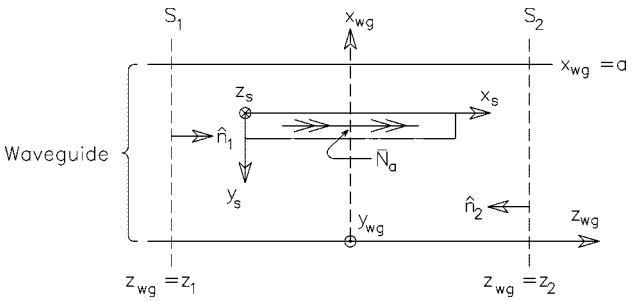

Fig. 5. The waveguide-to-slot interface. The current sheet $\bar{N}^b$ is located at S_1 or S_2.

We shall select $\bar{N}_b$ such that a single mode propagates in the positive direction of the z_{wg} axis for $z > z_1$ in Fig. 5. Hence,

$$\bar{N}^b = -2\hat{n}_1 \times (V\bar{e}e^{-jk_z z_1}) = -2V\bar{h}e^{-jk_z z_1} \tag{76}$$

where V is understood to be the voltage of a single TE or TM mode.

For $z > z_1$, the magnetic surface current $\bar{N}^b$ supports the magnetic field $\bar{H}^b$

$$\bar{H}^b = \frac{V}{Z_0}(\bar{h} + \hat{z}h_z)e^{-jk_z z} \tag{77}$$

We substitute (74)–(77) into (73). Using the orthogonality relation of [9, Sec. 8.1], we obtain

$$\begin{aligned} &\iint_{\mathrm{Aperture}} \frac{V}{Z_0}(\bar{h} + \hat{z}h_z)e^{-jk_z z} \\ &\quad \cdot \hat{z} \sum_{q=1}^{Q} V_q^{\mathrm{wg}} \sqrt{\frac{2}{l_s w_s}} \sin\left(\frac{q\pi}{l_s}\left(z + \frac{l_s}{2}\right)\right) dx\, dz \\ &= \iint_{S_1} \left(-I_{mn}^{e-}(\bar{h}_{mn}^e + \hat{h}_{z,mn}^e)e^{jk_z z}\right) \\ &\quad \cdot \left(-2V\bar{h}_{mn}^e e^{-jk_z z_1}\right) ds \end{aligned} \tag{78}$$

which may be written in the compact form

$$I_{mn}^{e-} = \sum_{q=1}^{Q} y_{mn}^{q-} V_q^{\mathrm{wg}} \tag{79}$$

where

$$\begin{aligned} y_{mn}^{q-} = \frac{1}{2Z_0}\sqrt{\frac{2}{l_s w_s}} \int_{\frac{-l_s}{2}}^{\frac{l_s}{2}} \int_{d-\frac{w_s}{2}}^{d+\frac{w_s}{2}} \\ h_{z,mn} e^{-jk_z z} \sin\left(\frac{q\pi}{l_s}\left(z + \frac{l_s}{2}\right)\right) dx\, dz. \end{aligned} \tag{80}$$

Hence, y_{mn}^{q-} is the ratio between the current I_{mn}^{e-} of the mnth mode propagating in the negative direction of the main waveguide z axis and the voltage V_q^{wg} of the qth TE_{q0} mode in the aperture of the slot.

Substituting h_z of (80) using (18) and (19) with $(m,n) = (1,0)$ and performing the indicated integrations yields

$$y_{10}^{q-} = \begin{cases} -j\sqrt{\dfrac{4}{abl_s w_s}}\dfrac{2q\pi}{l_s k_0 \eta}\cos\left(\dfrac{\pi}{a}d\right)\sin\left(\dfrac{\pi w_s}{2a}\right)\dfrac{\cos\left(\dfrac{k_z l_s}{2}\right)}{\left(\left(\dfrac{q\pi}{l_s}\right)^2 - k_z^2\right)}, \\ \qquad \text{when } q \text{ is odd} \\ \sqrt{\dfrac{4}{abl_s w_s}}\dfrac{2q\pi}{l_s k_0 \eta}\cos\left(\dfrac{\pi}{a}d\right)\sin\left(\dfrac{\pi w}{2a}\right)\dfrac{\sin\left(\dfrac{k_z l_s}{2}\right)}{\left(\left(\dfrac{q\pi}{l_s}\right)^2 - k_z^2\right)}, \\ \qquad \text{when } q \text{ is even.} \end{cases} \tag{81}$$

2) Scattered Waves in the Positive Direction of the $z_{\rm wg}$ Axis: Following a similar line of reasoning, we obtain

$$y_{10}^{q+} = \begin{cases} -j\sqrt{\dfrac{4}{abl_s w_s}}\dfrac{2q\pi}{l_s k_0 \eta}\cos\left(\dfrac{\pi}{a}d\right)\sin\left(\dfrac{\pi w_s}{2a}\right)\dfrac{\cos\left(\dfrac{k_z l_s}{2}\right)}{\left(\left(\dfrac{q\pi}{l_s}\right)^2 - k_z^2\right)}, \\ \qquad \text{when } q \text{ is odd} \\ -\sqrt{\dfrac{4}{abl_s w_s}}\dfrac{2q\pi}{l_s k_0 \eta}\cos\left(\dfrac{\pi}{a}d\right)\sin\left(\dfrac{\pi w_s}{2a}\right)\dfrac{\sin\left(\dfrac{k_z l_s}{2}\right)}{\left(\left(\dfrac{q\pi}{l_s}\right)^2 - k_z^2\right)}, \\ \qquad \text{when } q \text{ is even.} \end{cases} \tag{82}$$

3) Concluding Remarks: We may summarize the derivations made in this section by defining a slot to waveguide admittance $y_{mn}^{q\pm}$, which links the mode voltage of a TE_{q0} mode in the slot aperture facing the waveguide with the mnth mode current scattered in either direction of the main waveguide

$$I_{mn}^{e\pm} = \sum_{q=1}^{Q} y_{mn}^{q\pm} V_q^{\rm wg} \tag{83}$$

where

$$y_{10}^{q\pm} = \begin{cases} -j\sqrt{\dfrac{4}{abl_s w_s}}\dfrac{2q\pi}{l_s k_0 \eta}\cos\left(\dfrac{\pi}{a}d\right)\sin\left(\dfrac{\pi w_s}{2a}\right)\dfrac{\cos\left(\dfrac{k_z l_s}{2}\right)}{\left(\left(\dfrac{q\pi}{l_s}\right)^2 - k_z^2\right)}, \\ \qquad \text{when } q \text{ is odd} \\ \mp\sqrt{\dfrac{4}{abl_s w_s}}\dfrac{2q\pi}{l_s k_0 \eta}\cos\left(\dfrac{\pi}{a}d\right)\sin\left(\dfrac{\pi w_s}{2a}\right)\dfrac{\sin\left(\dfrac{k_z l_s}{2}\right)}{\left(\left(\dfrac{q\pi}{l_s}\right)^2 - k_z^2\right)}, \\ \qquad \text{when } q \text{ is even} \end{cases} \tag{84}$$

where the upper sign pertains to waves scattered in the positive direction and the lower sign pertains to waves scattered in the negative direction of the main waveguide.

G. Normalization of Scattering Parameters

The numbering of the four-ports of the coupler are as indicated in Fig. 3. The reference planes are located at $x_l = 0$ for ports 1 and 2 and at $z_{\rm wg} = 0$ for ports 3 and 4. For normalization purposes, the power incident in the waveguide and the strip line are computed. For the waveguide, we obtain [9, Sec. 8.1]

$$P_{\rm wg} = \frac{(1\ \mathrm{V})^2}{Z_{10}^{\rm TE}} = (1\ \mathrm{V})^2 \frac{k_z}{\omega\mu}. \tag{85}$$

For the strip line, we integrate the Poynting's vector between the ground planes on the surface $x_l = 0$. The numerical integration is performed in the spectral domain [12]

$$\begin{aligned} P_l &= \frac{1}{2}\,\mathrm{Re}\int_{-\infty}^{\infty}\int_0^h \hat{x}\cdot(\bar{E}\times\bar{H}^*)\,dz\,dy \\ &= \frac{1}{4\pi}\mathrm{Re}\int_{-\infty}^{\infty}\int_0^h \left(\tilde{G}_{yx}^{EK}\tilde{G}_{zx}^{*HK} - \tilde{G}_{zx}^{EK}\tilde{G}_{yx}^{*HK}\right)dz \\ &\quad \tilde{k}_{l,x}(k_y)\tilde{k}_{l,x}^*(k_y)\,dk_y \end{aligned} \tag{86}$$

where all elements of the spectral-domain Green's dyads are functions of $(-k_e, k_y, z)$.

1) S_{n1} Parameters: In order to derive the S_{n1} parameters, we apply the incident current of (20) $\bar{K}^{\rm inc}$ on port 1, while the waveguide mode $\bar{H}_{\rm wg}^{\rm inc}$ incident on port 3 (and 4) is left out. With all i_s^p elements equal to zero, we solve (65). We then obtain

$$\begin{aligned} &(S_{11}, S_{21}, S_{31}, S_{41}) \\ &\quad = \left(R, T, \sqrt{\frac{Z_{10}^{\rm TE}}{P_l}}\sum_{q=1}^{Q} y_{10}^{q-} V_q^{\rm wg}, \sqrt{\frac{Z_{10}^{\rm TE}}{P_l}}\sum_{q=1}^{Q} y_{10}^{q+} V_q^{\rm wg}\right). \end{aligned} \tag{87}$$

2) S_{n3} Parameters: In order to derive the S_{n1} parameters, we apply the incident waveguide mode $\bar{H}_{\rm wg}^{\rm inc}$ on port 3, while the incident current on port 1 (and 2) is left out. With all i_l^p, v_l^r, and v_l^s elements equal to zero, we solve (65). We then obtain

$$\begin{aligned} &(S_{13}, S_{23}, S_{33}, S_{43}) \\ &\quad = \left(\sqrt{\frac{P_l}{P_{\rm wg}}}R, \sqrt{\frac{P_l}{P_{\rm wg}}}T, \frac{Z_{10}^{\rm TE}}{1\ \mathrm{volt}}\sum_{q=1}^{Q} y_{10}^{q-} V_q^{\rm wg}, \right. \\ &\qquad \left. 1 + \frac{Z_{10}^{\rm TE}}{1\ \mathrm{volt}}\sum_{q=1}^{Q} y_{10}^{q+} V_q^{\rm wg}\right) \end{aligned} \tag{88}$$

The remaining S_{n2} and S_{n4} elements are readily obtained using reciprocity and the geometrical symmetry of the coupler.

III. Results

1) Geometry: To validate the electromagnetic model, an experimental coupler containing the waveguide-to-strip-line coupler was built. In Fig. 6, a photograph of the individual parts comprising the experimental coupler is shown. In Fig. 7, the position of the vias with respect to the strip line, aperture, and waveguide is shown. In Fig. 8, the cross section of the dielectric layers is shown with the location of the strip line indicated. Table I contains the relevant geometrical data. Note that the cross section of the slot used in the experimental coupler is,

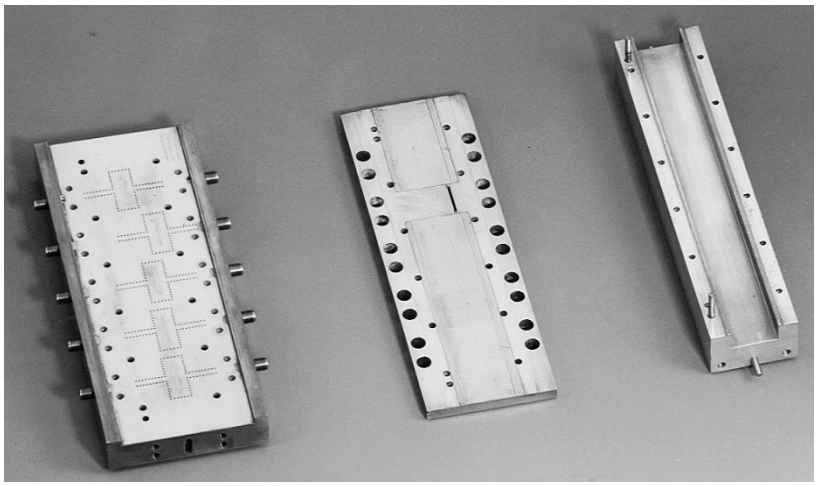

Fig. 6. Experimental waveguide-to-strip-line coupler.

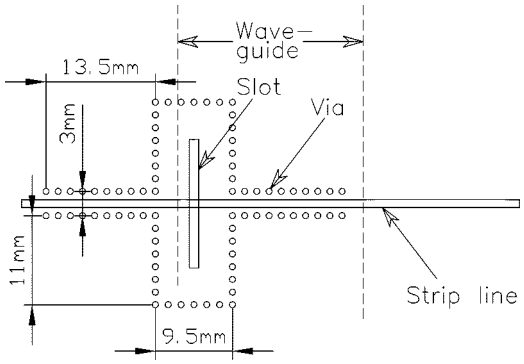

Fig. 7. Position of vias.

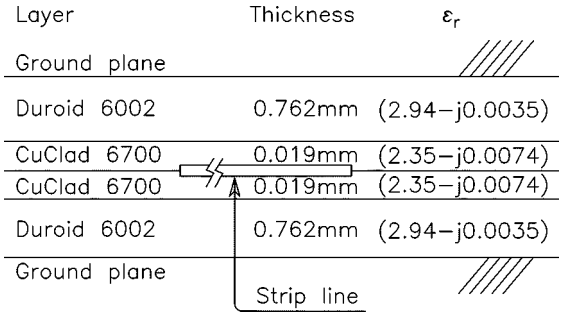

Fig. 8. Cross section of dielectric layers.

TABLE I
GEOMETRICAL DATA OF THE WAVEGUIDE-TO-STRIP LINE COUPLER

$a = 22.86$ mm	$b = 11.16$ mm	$d = 2.00$ mm
$t_s = 6.00$ mm	$w_s = 1.17$ mm	$l_s = 15.90$ mm
$t_l = 17$ μm	$w_l = 986$ μm	
$r_v = 375$ μm	$h = 1.56$ mm	$V = 78$

in fact, rectangular. First, a rounded-end slot has been milled. Second, the slot ends have been reamed using a broach blade into their final right-angled shape.

2) Measurements: The location of the reference planes (as defined in Section II-G) implies that the waveguide and strip line losses are to be extracted from the measurements in order to compare with the computed scattering parameters obtained using the electromagnetic model. Therefore, the following measurements have been made.

1) Prior to measuring the coupler, the inner surface of the waveguide containing the slot have been covered by conductive copper tape, leaving a 20-mm section open in the vicinity of the slot. Hence, the waveguide losses become identical in the present item and in item 2. All six combinations of two-port measurements have been made using an HP8722D network analyzer. For the port (1, 2) and (3, 4) measurements, standard two-port calibration in 3.5 mm and X-band waveguide have been applied, respectively. For the port (1, 3) (1, 4), (2, 3), and (2, 4) measurements, the so-called adapter removal calibration [14] has been applied.
2) The waveguide losses have been measured with the inner surface of the waveguide containing the slot fully covered by copper tape and with a 20-mm section left open at a location without the presence of the slot.
3) The connector losses are obtained from reflection measurements on shorted SMA ports (port 1 and 2). The measurements have been made directly on the connector of the network analyzer. Hence, no cables were involved.
4) The combined SMA connector and and strip-line losses have been measured with the slot in the ground plane of the strip-line circuit covered by copper tape.

Using the measurements of items 2–4, the lumped loss of the connectors, lumped loss the copper tape/no copper tape transitions (within the waveguide), and loss factors, i.e., α of $e^{-\alpha l}$, of the strip line and of the waveguide, respectively, were quantified. These lumped and distributed losses have been extracted from the measurements of item 1.

3) Refinements of the Electromagnetic Model: The finite thickness of the strip line t_l has been included in the analysis using Wheeler's formulation [15] providing a correction term Δw_l to the width of an equivalent zero thickness strip line.

As the vias are closely spaced (see Fig. 7), the electromagnetic field inside the cavity (formed by the ground planes and vias) is nonzero, while the electromagnetic field outside the

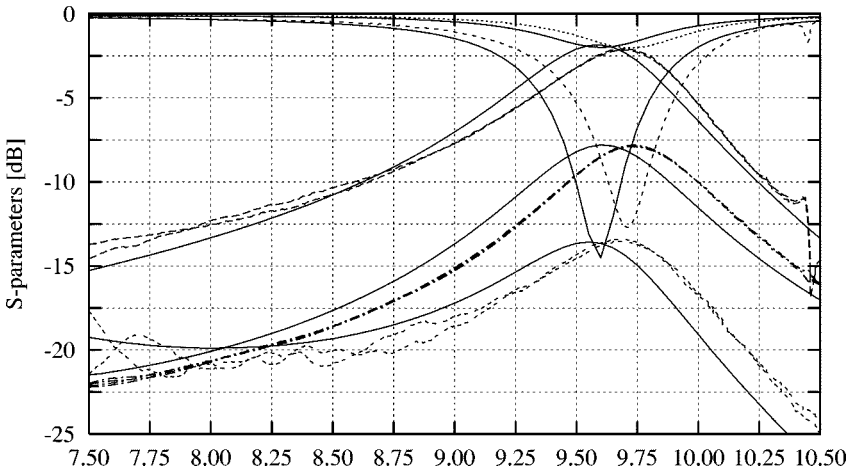

Fig. 9. Computed (S) and measured (M) scattering parameters of the coupler. "Center of current" displacement not applied.

cavity tends toward zero. Accordingly, we will encounter that the electric current on a via will be nonzero on the part of its surface facing the inside of the cavity, while the current on the part of its surface facing the outside of the cavity will be zero.

As a first-order approximation, we, therefore, assume the following θ dependence of the surface current of a via located with its symmety axis conincident with the z axis of a circular cylindrical coordinate system and with the x axis pointing toward the slot:

$$K_v(\theta) = \begin{cases} \cos\theta, & \text{if } |\theta| \le \dfrac{\pi}{2} \\ 0, & \text{if } \dfrac{\pi}{2} < |\theta| \le \pi. \end{cases} \tag{89}$$

We shall define the "center of current" (i.e., cc), in analogy with the center of gravity concept as follows:

$$\bar{r}_{\rm cc} = \frac{\int_{-\pi}^{\pi} K_v(\theta)(\hat{x}\cos\theta + \hat{y}\sin\theta)\, d\theta}{\int_{-\pi}^{\pi} K_v(\theta)\, d\theta} r_v. \tag{90}$$

Substitution of (89) in (90) yields

$$\bar{r}_{\rm cc} = \hat{x}\frac{\pi}{4} r_v. \tag{91}$$

For this study, the consequence of neglecting the θ dependence of the via current is that the cavity becomes electrically slightly oversized. Computed data confirms this, as the resonance frequency is 125 MHz, i.e., 1.3%, off the measured resonance frequency of the experimental coupler.

As an alternative to modifying the expansion functions used for the currents on the vias, we have chosen to decrease the size of the cavity by artificially moving all vias. The upper row (of vias) and the upper part of the cutoff section are displaced downwards, the right-hand-side column is displaced to the left-hand side and the remaining vias are displaced such that point symmetry with respect to the center of the slot is maintained. Using a displacement of 275 μm ensures perfect agreement between the computed and measured resonance frequencies. We appreciate that 275 μm is in close agreement with the $r_v\pi/4 = 295$ μm center of current.

4) Convergence and Consistency Aspects: Due to the use of expansion functions, which provide the proper edge conditions for the strip line and slot currents, as well as the proper current and charge distributions on the vias at the interface between the dielectric layers/ground planes, the numerical solution converges rapidly in terms of the number of expansion functions used. For the computations presented in this paper, $k_{l,x}(y)$ is a weighted sum of four Maxwellian modes [12], $I = 15$, $L = 4$, $M = 0$, $V = 78$, and $Q = 9$.

All possible checks involving reciprocity among the elements of the matrix in (65) agrees. Further, the conditions for the scattering parameters of a dissipationless and reciprocal four-port are fulfilled.

5) Computed Scattering Parameters: In Fig. 9, the computed (without moving the vias) and measured scattering parameters for the coupler is shown. Note that $|S_{11}| = |S_{21}|$, $|S_{12}| = |S_{22}|$, $|S_{13}| = |S_{14}| = |S_{23}| = |S_{24}| = |S_{31}| = |S_{32}| = |S_{41}| = |S_{42}|$, $|S_{33}| = |S_{44}|$, and $|S_{34}| = |S_{43}|$.

In Fig. 10, the computed (with the vias moved according to the "center of current" concept) and the measured scattering parameters for the coupler is shown. The agreement between the computed and measured scattering parameters of Fig. 10 is within the measurement accuracy, except for the S_{11}, S_{12}, S_{21}, and S_{22} parameters. We expect the discrepancy to be due to the $z^{r,vlm}$, $z^{s,\rm ref}$, $z^{s,\rm tr}$, $z^{s,i}$, and v_l^s inner products, i.e., the direct coupling between the vias and line, being set equal to zero. This may also explain that the resonance apparent at 10.45 GHz is not predicted.[2]

The experimental coupler couples –8 dB in two ports, which may be combined into –5 dB. Investigations prove that use of the slot offset is not feasible for an increase of the coupling. Stronger coupling may be obtained by matching the difference mode scattered off the slot onto the strip line by altering the strip line into a matching circuit (see Fig. 11). Weaker coupling is obtained by moving the slot toward the center of the broad side of the waveguide.

In Fig. 12, the currents (which are virtually identical in all layers) on each individual via is shown. The currents have been normalized with respect to the maximum current that flows on the four vias being located closest to the center of the slot. The height of a cylinder indicates the computed and normalized

[2]In [4], a similar resonance was attributed to the vias.

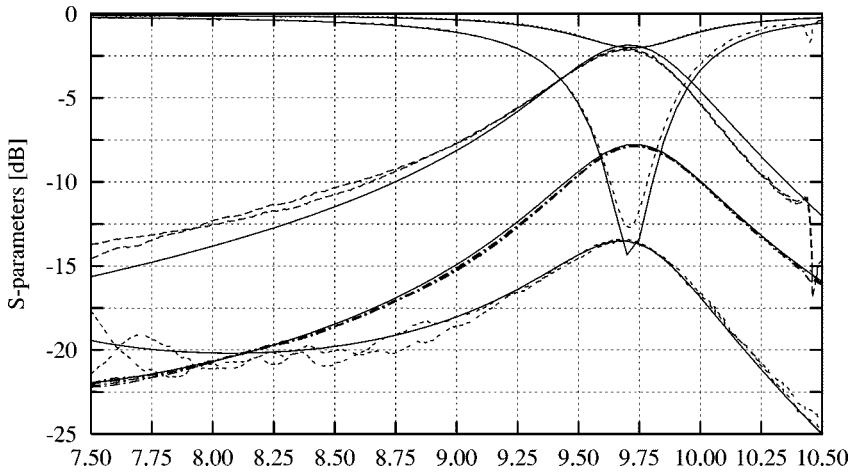

Fig. 10. Computed (S) and measured (M) scattering parameters of the coupler. "Center of current" displacement of 275 μm applied.

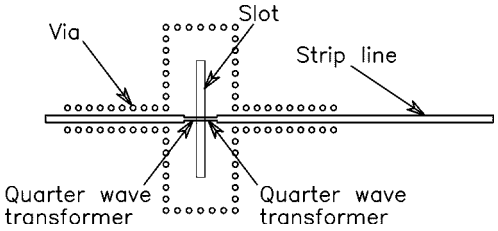

Fig. 11. Strip-line matching circuit for increased coupling.

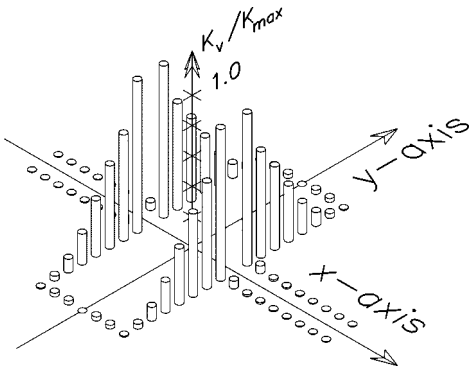

Fig. 12. Computed amplitude of via currents at resonance, i.e., $f = 9.75$ GHz. The source is an incident TE_{10} mode in the waveguide, i.e., $i_s^p \neq 0, i_l^p = v_l^r = v_l^s = 0$.

amplitude of the current on the co-located via. A linear scale has been applied. The resonance of the cavity and the waveguide cutoff effect of the two sections along the strip line is visible.

IV. Conclusion

In this paper, the waveguide-to-strip-line coupler has been described theoretically. The description is based on an integral-equation model for the problem where a space-domain formulation has been applied for the waveguide and slot regions and a spectral-domain formulation has been applied for the strip-line region. The notation applied for the involved coupling terms facilitates a network interpretation using admittances (impedances), as well as voltage and current generators.

Refinements to the integral-equation model have been discussed and have been implemented. The so-called "center of current" concept is shown to improve the predicted resonance frequency of the coupler. Future improvements of the electromagnetic model may include the azimuthal variation of the current on the surface of the vias. Investigations of this kind are underway.

Computed and measured scattering parameters are in excellent agreement. The computed and measured scattering parameters corresponding to the coupling terms, i.e., S_{31}, etc., agree within 0.1 dB at the resonance frequency.

Computed data for the currents on the vias demonstrate that the vias surrounding the slot operates as four sides of a cavity. Also, the cutoff operation of the vias located along the strip line is demonstrated.

In summary, this paper has described a theoretically well-founded electromagnetic model that enables accurate design of practical waveguide-to-strip-line couplers.

Acknowledgment

The author thanks T. L. Elmkjær for his help with the derivations necessary for the electromagnetic model and, in particular, for the derivations concerned with the waveguide self admittance, A. K. Thomsen and J. Granholm for their help with the design, calibration and measurement of the experimental coupler, Dr. U. V. Gothelf for his help with the method of moments code, Dr. M. Dich for his help with waveguide issues, and finally, Prof. J. E. Hansen for his encouragement throughout this work and for his contributions to this paper.

References

[1] R. J. Mailloux, "Antenna array architecture," *Proc. IEEE*, vol. 80, pp. 163–172, Jan. 1992.
[2] H. A. Bethe, "Theory of diffraction by small holes," *Phys. Rev.*, no. 66, pp. 163–182, 1944.
[3] H. Perini and P. Sferrazza, "Rectangular waveguide to strip transmission line directional couplers," in *IRE Wescon Conv. Rec.*, 1957, pp. 16–21.
[4] J. Kassner and W. Menzel, "An electromagnetically coupled package feed-through structure for multilayer carrier substrates," in *28th European Microwave Conf.*, vol. 2, Amsterdam, The Netherlands, Oct., 6–8 1998, pp. 428–432.
[5] A. Østergaard, "Spectral domain integral equation model of a probe feed microstrip antenna," Ph.D. dissertation, Dept. Electromag. Syst., Tech. Univ. Denmark, Lyngby, Denmark, Dec. 1994.

[6] Y. Rahmat-Samii, "On the question of computation of the dyadic Green's function at the source region in waveguides and cavities," *IEEE Trans. Microwave Theory Tech.*, vol. MTT-23, pp. 762–765, Sept. 1975.
[7] P. Slättman and A. Østergaard, "A study of an electric field integral equation in the space domain for layered media," Dept. Electromag. Syst., Tech. Univ. Denmark, Lyngby, Denmark, Tech. Rep. R594, Sept. 1994.
[8] A. Østergaard, "An algorithm for numerical computation of dyadic Green's functions in multi layered media," ESA/ESTEC Electromag. Div., Noordwijk, The Netherlands, ESTEC Working Paper 1709, Feb. 1993.
[9] R. F. Harrington, *Time Harmonic Electromagnetic Fields* , ser. (McGraw-Hill Elect. Electron. Eng. Series) . New York: McGraw-Hill, 1961.
[10] R. W. Jackson and D. M. Pozar, "Full-wave analysis of microstrip open-end and gap discontinuities," *IEEE Trans. Microwave Theory Tech.*, vol. MTT-33, pp. 1036–1042, Oct. 1985.
[11] T. Itoh, Ed., *Numerical Techniques for Microwave and Milimeter-Wave Passive Structures*. New York: Wiley , 1989, ch. 5.
[12] U. V. Gothelf and A. Østergaard, "Full wave analysis of a two slot microstrip filter using a new algorithm for computation of the spectral integrals," *IEEE Trans. Microwave Theory Tech.*, vol. 41, pp. 101–108, Jan. 1993.
[13] C. A. Balanis, *Antenna Theory—Analysis and Design*, 2nd ed. New York: Wiley, 1997.
[14] "Measuring Noninsertable Devices," Hewlett-Packard Company, Englewood, NJ, Tech. Rep. 8510-13, 1997.
[15] H. A. Wheeler, "Transmission-line properties of a strip line between parallel plates," *IEEE Trans. Microwave Theory Tech.*, vol. MTT-26, pp. 866–876, Nov. 1978.

Allan Østergaard was born in Denmark, on May 10, 1963. He received the M.Sc. and Ph.D. degrees in electrical engineering from the Technical University of Denmark (TUD), Lyngby, Denmark, in 1987 and in 1994 respectively.

In 1987, he joined the Department of Electromagnetic Systems (EMI) (formerly the Electromagnetics Institute), TUD, where he developed high-speed digital circuitry for an airborne SAR system. In 1993, he joined the Antenna Section, Electromagnetics Division, European Space Agency, Noordwijk, The Netherlands, where he was involved with full-wave analysis of multilayer structures and with design of offset reflector antennas. In 1994, he returned to EMI as an Associate Research Professor until he joined the TERMA Elektronik AS, Lystrup, Denmark, in 1997, where he is currently a Senior Antenna Engineer involved with antennas for pulsed microwave radar systems. His research interests are in the field of electromagnetic modeling and numerical analysis of multilayer circuits and antennas.